Retinal Image Analysis with Shearlets

Francesco Levet[1], Miguel A. Duval-Poo[2], Ernesto De Vito[2] and Francesca Odone[1]

[1]Dipartimento di Informatica Bioingegneria Robotica e Ingegneria dei Sistemi (DIBRIS), Università degli Studi di Genova, 16146 Genova, Italy
[2]Dipartimento di Matematica (DIMA), Università degli Studi di Genova, 16146 Genova, Italy

Abstract

In this paper we propose a method for segmenting blood vessels in retinal images based on the shearlet transform. Shearlets are a relatively new directional multi-scale framework for signal analysis, which have been shown effective to enhance signal discontinuities such as edges and corners at multiple scales. The algorithm we propose builds on the idea of enhancing ridge-like structures at different scales by computing the shearlet transform with an appropriate mother function, the mexican hat wavelet. This allows us to detect precisely structures of different widths. We provide an experimental analysis of our approach on a benchmark dataset and we show very good performances in comparison with other multi-resolution methods from the state of the art.

1. Introduction

The segmentation of blood vessels from a retinal image plays a key role in assessing the vessels morphological properties such as length, width, tortuosity and/or branching pattern and angles. These properties are wildly used for the diagnosis, treatment, and evaluation of various cardiovascular and opthalmologic diseases such as diabetes, hypertension, arteriosclerosis among others [KB11].

In a nutshell, the process of blood vessel segmentation consists in generating a binary mask in which pixels are labeled as vessel or background. The goal is to capture as much detail (fine vessels) as possible, simultaneously avoiding false positives and, ideally, preserving the vessel connectivity.

Many approaches for automated vessel segmentation have been reported in the literature over the years. In a recent survey [FRH*12], those methods have been divided into six main categories; (i) pattern recognition techniques, (ii) matched filtering, (iii) vessel tracking/tracing, (iv) mathematical morphology, (v) multi-scale approaches, (vi) model based approaches and (vii) parallel/hardware based approaches. Of our special interest are multi-scale image representations, where the idea is to better extract blood vessels having varying width at different scales [MPHS*99, MPHT*07, MPHTP07, ABPS08, FHK*08, VD10].

In this work, we address the problem of detecting and segmenting the blood vessel in a retinal image by using the fast finite shearlet transform [HS14]. Contrary to the traditional wavelets, shearlets are capable to efficiently capture the anisotropic information in multivariate problem classes. They have been shown effective to enhance signal discontinuities such as edges [YLEK09, DPODV15a], corners [DPODV15b] and also isotropic features like blobs [DPNODV16] at multiple scales. The vessel segmentation

algorithm we propose builds on the idea of enhancing ridge-like structures in the image at multiple scales. We define a *ridgeness* measure $\mathcal{R}$ associated with each pixel at a given scale and normalized with respect to each scale considered. Then we obtain a binary map of vessel/background points by means of a hysteresis thresholding. Notice that we also exploit the sparseness property of the shearlet transform in a first noise removal phase. Our algorithm is elegant and effective, and produces accurate segmentations. We experimentally assess it on the DRIVE dataset where we show very good performances in comparison with other multi-resolution methods.

The remainder of this paper is organized as follows: in Section 2 we review the fast finite shearlet transform. Section 3 propose the blood vessel segmentation method based on shearlets. Section 4 reports the experimental results of the proposed method on the DRIVE dataset. Section 5 is left to a final discussion.

2. The Fast Finite Shearlet Transform

The shearlet transform can be computed by different implementations [YLEK09, KSZ12, KL12, KKL12, KLZ12, EL12]. Motived by previous results for edge and corner detection [DPODV15a], we use the Fast Finite Shearlet Transform (FFST) introduced in [HS14] whose definition we briefly recall.

Let $\mathcal{I}$ be an image of size $N_1 \times N_2$, where $(0,0)$ $(0,N_2-1)$ and $(N_1-1,0)$ denote left-bottom, left-top and right-bottom corners, respectively. The FFST of $\mathcal{I}$ (with j_0 scales) is defined as

$$\mathcal{SH}(\mathcal{I})(j,k,m) = \begin{cases} \langle \mathcal{I}, \psi^{\mathrm{h}}_{j,k,m} \rangle \\ \langle \mathcal{I}, \psi^{\mathrm{v}}_{j,k,m} \rangle \\ \langle \mathcal{I}, \phi_m \rangle \end{cases} \quad (1)$$

where $j = 0, \ldots, j_0 - 1$ labels the (coarse-to-fine) scales, the index $k = -\lfloor 2^{j/2} \rfloor, \ldots, \lfloor 2^{j/2} \rfloor$ parametrizes the shearing transforms, and $m = (m_1, m_2)$ is associated with translations, $m_1 \in \{0, \ldots, N_1 - 1\}$, $m_2 \in \{0, \ldots, N_2 - 1\}$. In the right side of Eq. (1) $\langle \cdot, \cdot \rangle$ denotes the Euclidean scalar product in $\mathbb{R}^{N_1 \times N_2}$, the filters $\psi_{j,k,m}^{h,v}$ are the horizontal and vertical shearlets

$$\psi_{j,k,m}^{h,v}(n_1, n_2) = 2^{-3j/4} \psi^{h,v}(x_1, x_2) \tag{2}$$
$$x_1 = 2^j (n_1 - m_1)/N_1 + k 2^{j/2}(n_2 - m_2)/N_2$$
$$x_2 = 2^{j/2}(n_2 - m_2)/N_2$$

with $n_1 = 0, \ldots, N_1 - 1$, $n_2 = 0, \ldots, N_2 - 1$ (see Fig. 1 showing the behavior in the Fourier domain). Note that, in space, a shearing k leaves the horizontal lines invariant, whereas vertical lines are rotated around the intersection with the x-axis to have direction $(k, 1)$. Hence the shearing parameter k labels the orientations and, in the following, we refer to k as the orientation direction.
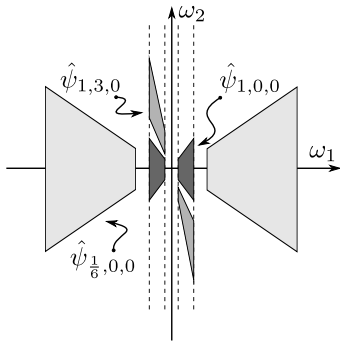

Figure 1: Support of the shearlets $\hat{\psi}_{j,k,m}^h$ (in the frequency domain) for different values of j and k.

The generating function $\psi^h \in L^2(\mathbb{R}^2)$ factorizes in the Fourier domain as

$$\hat{\psi}^h(\omega_1, \omega_2) = \begin{cases} \hat{\psi}_1(\omega_1) \hat{\psi}_2\left(\frac{\omega_2}{\omega_1}\right) & |\omega_2/\omega_1| \leq 1, |\omega_1| \geq 1 \\ 0 & \text{otherwise,} \end{cases}$$

where the function $\hat{\psi}_1$ is a 1D-dimensional wavelet and $\hat{\psi}_2$ is a 1D bump function, see Fig. 2. The specific choice of ψ_1 and ψ_2 influences the class of local features that are enhanced by the shearlet transform (see Sect. 3.1). The function ψ^v is defined in a similar way by interchanging ω_1 and ω_2. The filters ϕ_m (with m ranging as above) are generated by translation of a suitable scaling function ϕ,

$$\hat{\phi}_m(\omega_1, \omega_2) = \hat{\phi}(\omega_1, \omega_2) e^{-2\pi i \left(\frac{\omega_1 m_1}{N_1} + \frac{\omega_2 m_2}{N_2}\right)}$$

and they provide a coarse scale system associated with the low frequency region. The fast finite shearlet transform can be efficiently computed by applying the 2D fast Fourier transform (`fft`) and its inverse (`ifft`). With respect to the original implementation in [HS14] we use a dyadic scale 2^{-j} instead of 4^{-j} to reduce the gap between consecutive scales.
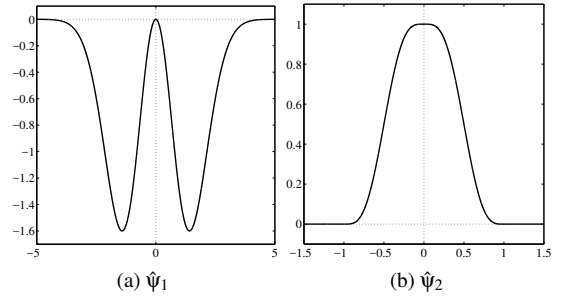

Figure 2: The Mexican hat wavelet $\hat{\psi}_1$ and the bump function $\hat{\psi}_2$ in the Fourier domain.

3. Blood Vessel Segmentation with Shearlets

Blood vessels (arteries and veins) appear in a retinal image as elongated features in a wide range of widths (see Fig. 3). Arteries transport blood rich in oxygen therefore they appear brighter in the image, while veins are visualized barker since they transport the blood at a low oxygen level. The central reflex (the light reflex of the inner parts of the vessels) is wider in arteries and smaller in veins.

Due to their characteristic, blood vessels can be detected as ridge features. In image processing ridges are points for which the main principal curvature assumes a maximum (minimum) in the main principal curvature direction [Har83].

Figure 3: Classification of blood vessels in a retinal image. Veins (1) and Arteries (2).

As we can observe in Fig. 3, the width of a vessel decreases gradually as it travels outward from the optic disk. Thus, the use of a multi-scale representation of the image seems natural for the blood vessels detection.

3.1. Scale Selection with Shearlets

Multi-scale frameworks, like scale-space, wavelets and shearlets, represent image structures at multiple scales and are thus appropriate for detecting structures or features with different spatial extent.

Lindeberg showed in his seminal works [Lin98b, Lin98a] that the detection of local maxima over scales of normalized differential entities provides a consistent framework for generating hypothesis about local appropriate scales for detecting image features such as blobs, corners, edges and ridges. Furthermore, that ridges have

the characteristic property that the selected scales on a scale-space ridge reflect the width of the ridge.

In this section, we show how shearlet coefficients can detect the correct scale of ridge features while providing directional information. We stress that the choice of $\hat{\psi}_1$ and $\hat{\psi}_2$ influences the type of local features that are enhanced by the shearlet transform. Thus, in this work we made the same choice as in [DPNODV16] where $\hat{\psi}_1$ is the Mexican hat wavelet and $\hat{\psi}_2$ is a smooth function with compact support (see Fig. 2). With this selection, the authors in [DPN-ODV16] derived a measure which is very effective for blob-like features detection and that is closely related to the Laplacian of Gaussian. They also demonstrated that the measure satisfies the perfect scale invariance property in the continuous case.

In our work we use the same measure for detect ridge features of a retinal image at multiple scales. Formally, the $\mathcal{R}$ measure (as is going to be called in this work) is the scale-normalized sum of the fast finite shearlet transform coefficients across the shearing parameter,

$$\mathcal{R}(j,m) = 2^{\frac{5j}{4}} \sum_k \mathcal{SH}(\mathcal{I})(j,k,m), \qquad (3)$$

where j,k,m are the scaling, shearing and translation parameters. Fig. 4 shows the $\mathcal{R}$ measure of a retinal image at different scales.

Notice that this measure will serve our purposes of segmenting the ridge features, since at their appropriate scales, ridges can be approximated by the second derivative of a Gaussian without taken into account the central reflex of the blood vessel and thus obtain a complete enhancement of the blood vessel.

Finally, blood vessels can be simply identified as those points m in the intensity image that assumes a maximum over scales on the the $\mathcal{R}$ measure,

$$\mathcal{S}(m) = max_j \mathcal{R}(j,m). \qquad (4)$$

3.2. The Shearlet Blood Vessel Segmentation Method

We now describe the proposed Shearlet Blood Vessel Segmentation (SBVS) method. The input of our method is a color retinal image, also known as fundus image, which is acquired by making photographs of the back of the eye. And the output is a binary image that represents the retinal vessel map.

The proposed method is composed of three main parts: (a) pre-processing (b) shearlet multi-scale analysis and (c) segmentation and post-processing.

Pre-processing. The first step is to convert the input color image to a intensity image. However, instead merging all the channels, a common practice in blood vessel segmentations methods is to select only the green channel since it exhibits the best vessel-background contrast.

Next the CLAHE (Contrast Limited Adaptive Histogram Equalization) operator is used to produce local contrast enhancement and also can reduce the undesired noise amplification of the retinal image [PAA*87].

Shearlet multi-scale analysis. We begin by computing the shearlet transform, Eq. (1), of the pre-possessed input image and then remove the noise from the image signal.

(a) $max_j\mathcal{R}$ (b) $max_j\mathcal{R}$ after hard thesholding
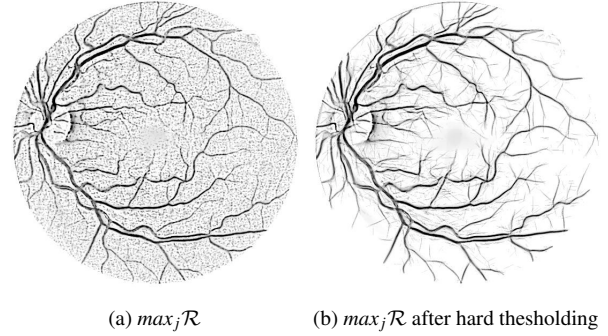
Figure 5: Example of noise removal using shearlets on a retinal image.

It is well known that sparse representations are very useful in decorrelating the image signal from the noise. This notion has been formalized in the classical wavelet shrinkage approach [DJ94], and has lead to the development of successful denoising methods. Shearlets have been shown to be highly effective in denoising images [ELL08, ELC09]. Compared to classical wavelets, shearlets have the advantage to also perform the thresholding on the directional decomposition of the image and thus preserve the main direction of the features.

Therefore, in our method we remove the image noise by hard thresholding the shearlet coefficients at every position, scale and direction [ELL08],

$$\mathcal{SH}(\mathcal{I})(j,k,m) = \begin{cases} \mathcal{SH}(\mathcal{I})(j,k,m) & |\mathcal{SH}(\mathcal{I})(j,k,m)| \geq \tau_{j,k,m} \\ 0 & |\mathcal{SH}(\mathcal{I})(j,k,m)| < \tau_{j,k,m} \end{cases}$$
$$(5)$$

The threshold is given by $\tau_{j,k,m} = \sigma_{\eta j,k}^2 / \sigma_{j,k,m}^2$, where $\sigma_{\eta j,k}^2$ is the noise variance at scale j and shear k and $\sigma_{j,k,m}^2$ is the variance of the m-th coefficient at scale j and shear k. The variances $\sigma_{\eta j,k}^2$ are estimated by using a Monte-Carlo technique in which the variances are computed for several normalized noise images and then the estimates are averaged. Fig. 5 shows an example of noise removal using shearlets on a retinal image.

Once the shearlets coefficients are noise free, we compute the $\mathcal{R}$ measure (Eq. 3) and then we select the pixels values that are maximum over the scale dimension (Eq. 4).

Segmentation and post-processing. For segmenting the enhanced blood vessels from the rest of the image we binarize the obtained intensity image using hysteresis threshold [Can86]. This is a bi-threshold procedure typically used for two class object-background pixel segmentation. The blood vessel pixels with a value below the lower threshold or above the upper threshold are definitely removed or kept respectively. The other blood vessel pixels will be kept if they are next to those that have already been selected.

Finally, once he obtained the binary segmented image, we remove all small connected components that usually belongs to un-removed noise or some retina pathologies. The proposed method is
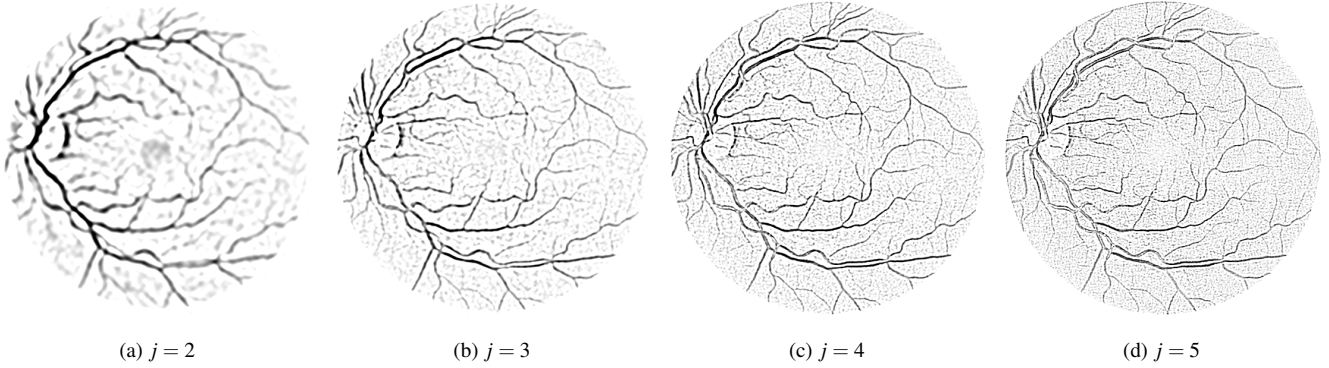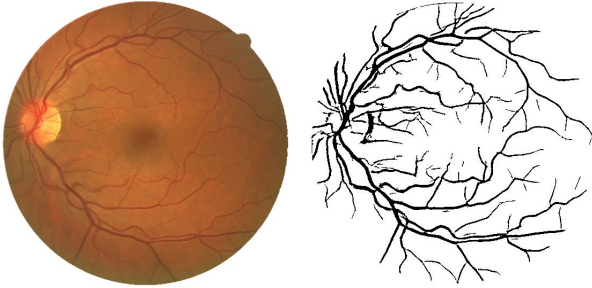
| (a) $j = 2$ | (b) $j = 3$ | (c) $j = 4$ | (d) $j = 5$ |

Figure 4: The $\mathcal{R}$ measure of a retinal image at different scales j.

Figure 6: Qualitative result of our method on a retinal image.

Algorithm 1 Shearlet Blood Vessel Segmentation (SBVS).

Input $\mathcal{I}$: retinal color image, j_0: number of scales.
Output $\mathcal{S}$: segmented binary image.
  procedure SBVS($\mathcal{I}, j_0$)
    /* *pre-processing* */
    $\mathcal{I}_G = $ get_green_channel($\mathcal{I}$);
    $\mathcal{I}_G = $ clahe($\mathcal{I}_G$);
    /* *shearlet multi-scale analysis* */
    $\mathcal{SH} = $ ffst($\mathcal{I}_G$);   ▷ /* *Eq. 1* */
    $\mathcal{SH} = $ remove_noise($\mathcal{SH}$);   ▷ /* *Eq. 5* */
    for $j = 0, \ldots, j_0 - 1$ **do**
        $\mathcal{R}(j,m) = 2^{\frac{5j}{4}} \sum_k \mathcal{SH}(j,k,m), \quad \forall m \in \mathcal{I}_G$
    end for
    $\mathcal{S} = \max_j(\mathcal{R}(j,m)), \quad \forall m \in \mathcal{I}_G$
    /* *segmentation and post-processing* */
    $\mathcal{S} = $ hysthresh($\mathcal{S}$);
    $\mathcal{S} = $ remove_cc($\mathcal{S}$);
    return $\mathcal{S}$;
  end procedure

---

summarized in Alg. 1, while Fig. 6 shows a qualitative result of our method on a retinal image.

4. Experimental Results

In this section we preset the experimental results obtained by using the proposed method on the well known DRIVE dataset [SAN*04].

DRIVE (Digital Retinal Images for Vessel Extraction) is a publicly dataset (available at http://www.isi.uu.nl/Research/Databases/DRIVE/) that consists of a total of 40 color JPEG compressed fundus images. The images were obtained from a diabetic retinopathy screening program in the Netherlands. The screening population consisted of 453 subjects between 31 and 86 years of age. Each image is captured using 8 bits per color plane at 768×584 pixels. The field of view (FOV) of each image is circular with a diameter of approximately 540 pixels. The images of the dataset have been cropped around the FOV. For each image, a mask image is provided that delineates the FOV. The set of 40 images was divided into a training and test set both containing 20 images. For the training images, a single manual segmentation of the blood vessels is available. For the test cases, two manual segmentations are available; one is used as a gold standard, the other one can be used to compare computer generated segmentations with those of an independent human observer. All human observers that manually segmented the blood vessels were instructed and trained by an experienced ophthalmologist. Fig. 7 shows the first retinal image of the DRIVE dataset.

The evaluation of blood vessel segmentation methods in retinal images is a pixel-based classification result, where any pixel of the segmented image is classified either as blood vessel or a surrounding tissue. There are four possibilities; two classifications and two misclassifications. The classifications are the true positive (TP) where a pixel is identified as a blood vessel in both the ground truth and segmented image, and the true negative (TN) where a pixel is classified as a non-vessel in the ground truth and the segmented image. The two misclassifications are the false negative (FN) where a pixel is classified as non-vessel in the output image but as a blood vessel pixel in the ground truth image, and the false positive (FP) where a pixel is marked as blood vessel in the segmented image but non-vessel in the ground truth image. In addition, the true positive rate (TPR) represents the fraction of pixels correctly detected as blood vessel pixels. The false positive rate (FPR) is the fraction of
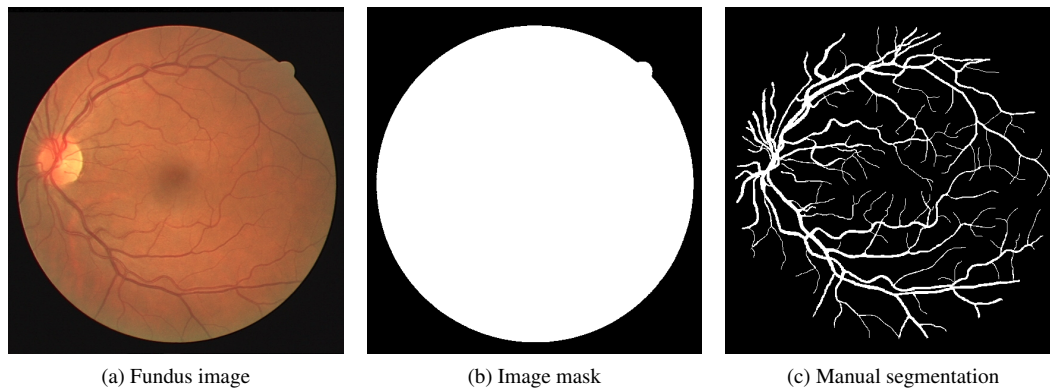
| (a) Fundus image | (b) Image mask | (c) Manual segmentation |

Figure 7: The first retinal image of the DRIVE dataset.

Method	SEN	SPE	ACC	AUC
Martinez et al. [MPHS*99]	0.639	-	0.918	-
Martinez et al. [MPHT*07]	0.725	0.965	0.934	-
Martinez et al. [MPHTP07]	0.660	0.961	0.922	-
Anzalone et al. [ABPS08]	-	-	0.942	-
Vlachos et al. [VD10]	0.747	0.955	0.929	-
SBVS (our approach)	**0.728**	**0.971**	**0.940**	**0.932**

Table 1: Comparison of multi-scale approaches for blood vessel segmentation on the DRIVE dataset.

pixels erroneously detected as blood vessel pixels. The commonly used performance metrics are the followings:

- *Accuracy (ACC)*. It is the ratio of the total number of correctly classified pixels (TP + TN) to the number of pixels in the image FOV.
- *Sensitivity (SEN)*. Reflects the ability of the algorithm to detect the vessel pixels: TP/(TP + FN).
- *Specificity (SPE)*. Reflects the ability to detect non-vessel pixels: TN/(TN + FP).

Another common way of evaluate the segmentation method performance is by plotting the *Receiver Operating Characteristic (ROC)* curve. This curve plots the fraction of blood vessel pixels correctly classified, namely the TPR, versus the fraction of non-vessel pixels wrongly classified as blood vessel, namely the FPR. The closer the curve approaches the top left corner, the better is the performance of the method. Figure 8 reports the ROC curve obtained by our algorithm on the DRIVE dataset. A frequently used performance measure extracted from the ROC curve is the value of the *Area Under the Curve (AUC)* which is 1 for an optimal method. Notice that for retinal images, the TPR and FPR are computed considering only pixels inside the FOV.

The proposed method SBVS is compared with other multi-scale algorithms. The results can be observed in Tab. 1. As we can observe our method obtain comparable, in occasions better, results with respect to other multi-scale blood vessel segmentation approaches.
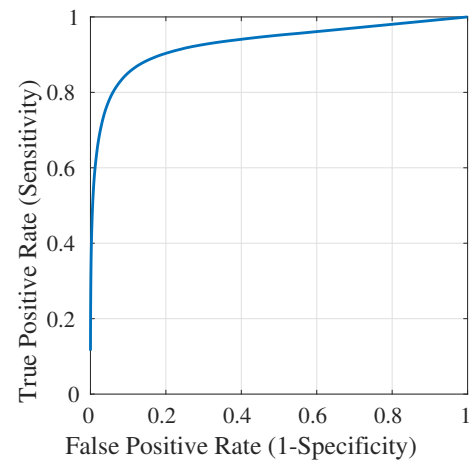

Figure 8: ROC curve of the proposed method for the DRIVE dataset.

5. Conclusions

We presented a method for retinal image analysis based on the shearlet transform. The method performs vessel segmentation in three main steps: preprocessing, multi-scale analysis, hysteresis thresholding. In the multi-scale analysis step, we compute the shearlet transform of an image, relying on the mexican hat wavelet which allows us to enhance ridge structures. We first exploit the spareness of the transform to perform noise removal. Then we compute, for each scale a map enhancing ridges, which we then merge in a final global map. Thanks to a hysteresis thresholding procedure we associate each pixel with a vessel / background label. Our method is elegant and effective and has the potential to provide further descriptive elements of the detected vessels to be used in future analysis tasks, such as measures of tortuosity or estimates of the vessel width; this will be the goal of future research.

References

[ABPS08] ANZALONE A., BIZZARRI F., PARODI M., STORACE M.: A modular supervised algorithm for vessel segmentation in red-free retinal

images. *Computers in biology and medicine 38*, 8 (2008), 913–922. 1, 5

[Can86] CANNY J.: A computational approach to edge detection. *Pattern Analysis and Machine Intelligence, IEEE Transactions on*, 6 (1986), 679–698. 3

[DJ94] DONOHO D. L., JOHNSTONE J. M.: Ideal spatial adaptation by wavelet shrinkage. *Biometrika 81*, 3 (1994), 425–455. 3

[DPNODV16] DUVAL-POO M. A., NOCETI N., ODONE F., DE VITO E.: Scale invariant interest points with shearlets. *arXiv preprint arXiv:1607.07639* (2016). 1, 3

[DPODV15a] DUVAL-POO M. A., ODONE F., DE VITO E.: Edges and corners with shearlets. *Image Processing, IEEE Transactions on 24*, 11 (2015), 3768–3780. 1

[DPODV15b] DUVAL-POO M. A., ODONE F., DE VITO E.: Enhancing signal discontinuities with shearlets: An application to corner detection. In *Image Analysis and Processing-ICIAP 2015*. Springer, 2015, pp. 108–118. 1

[EL12] EASLEY G. R., LABATE D.: Image processing using shearlets. In *Shearlets*. Springer, 2012, pp. 283–325. 1

[ELC09] EASLEY G. R., LABATE D., COLONNA F.: Shearlet-based total variation diffusion for denoising. *Image Processing, IEEE Transactions on 18*, 2 (2009), 260–268. 3

[ELL08] EASLEY G., LABATE D., LIM W.-Q.: Sparse directional image representations using the discrete shearlet transform. *Applied and Computational Harmonic Analysis 25*, 1 (2008), 25–46. 3

[FHK*08] FARNELL D. J., HATFIELD F., KNOX P., REAKES M., SPENCER S., PARRY D., HARDING S.: Enhancement of blood vessels in digital fundus photographs via the application of multiscale line operators. *Journal of the Franklin institute 345*, 7 (2008), 748–765. 1

[FRH*12] FRAZ M. M., REMAGNINO P., HOPPE A., UYYANONVARA B., RUDNICKA A. R., OWEN C. G., BARMAN S. A.: Blood vessel segmentation methodologies in retinal images–a survey. *Computer methods and programs in biomedicine 108*, 1 (2012), 407–433. 1

[Har83] HARALICK R. M.: Ridges and valleys on digital images. *Computer Vision, Graphics, and Image Processing 22*, 1 (1983), 28–38. 2

[HS14] HÄUSER S., STEIDL G.: Fast finite shearlet transform. *arXiv preprint arXiv:1202.1773v2* (2014). 1, 2

[KB11] KANSKI J. J., BOWLING B.: *Clinical ophthalmology: a systematic approach*. Elsevier Health Sciences, 2011. 1

[KKL12] KITTIPOOM P., KUTYNIOK G., LIM W.-Q.: Construction of compactly supported shearlet frames. *Constructive Approximation 35*, 1 (2012), 21–72. 1

[KL12] KUTYNIOK G., LABATE D.: *Shearlets: Multiscale analysis for multivariate data*. Springer, 2012. 1

[KLZ12] KUTYNIOK G., LIM W.-Q., ZHUANG X.: Digital shearlet transforms. In *Shearlets*. Springer, 2012, pp. 239–282. 1

[KSZ12] KUTYNIOK G., SHAHRAM M., ZHUANG X.: Shearlab: A rational design of a digital parabolic scaling algorithm. *SIAM Journal on Imaging Sciences 5*, 4 (2012), 1291–1332. 1

[Lin98a] LINDEBERG T.: Edge detection and ridge detection with automatic scale selection. *International Journal of Computer Vision 30*, 2 (1998), 117–156. 2

[Lin98b] LINDEBERG T.: Feature detection with automatic scale selection. *International journal of computer vision 30*, 2 (1998), 79–116. 2

[MPHS*99] MARTÍNEZ-PÉREZ M. E., HUGHES A. D., STANTON A. V., THOM S. A., BHARATH A. A., PARKER K. H.: Retinal blood vessel segmentation by means of scale-space analysis and region growing. In *International Conference on Medical Image Computing and Computer-Assisted Intervention* (1999), Springer, pp. 90–97. 1, 5

[MPHT*07] MARTINEZ-PEREZ M. E., HUGHES A. D., THOM S. A., BHARATH A. A., PARKER K. H.: Segmentation of blood vessels from red-free and fluorescein retinal images. *Medical image analysis 11*, 1 (2007), 47–61. 1, 5

[MPHTP07] MARTINEZ-PEREZ M. E., HUGHES A. D., THOM S. A., PARKER K. H.: Improvement of a retinal blood vessel segmentation method using the insight segmentation and registration toolkit (itk). In *2007 29th Annual International Conference of the IEEE Engineering in Medicine and Biology Society* (2007), IEEE, pp. 892–895. 1, 5

[PAA*87] PIZER S. M., AMBURN E. P., AUSTIN J. D., CROMARTIE R., GESELOWITZ A., GREER T., TER HAAR ROMENY B., ZIMMERMAN J. B., ZUIDERVELD K.: Adaptive histogram equalization and its variations. *Computer vision, graphics, and image processing 39*, 3 (1987), 355–368. 3

[SAN*04] STAAL J., ABRÀMOFF M. D., NIEMEIJER M., VIERGEVER M. A., VAN GINNEKEN B.: Ridge-based vessel segmentation in color images of the retina. *IEEE transactions on medical imaging 23*, 4 (2004), 501–509. 4

[VD10] VLACHOS M., DERMATAS E.: Multi-scale retinal vessel segmentation using line tracking. *Computerized Medical Imaging and Graphics 34*, 3 (2010), 213–227. 1, 5

[YLEK09] YI S., LABATE D., EASLEY G. R., KRIM H.: A shearlet approach to edge analysis and detection. *Image Processing, IEEE Transactions on 18*, 5 (2009), 929–941. 1